RADC-TR-76-56
Technical Report
April 1976

ADA025185

MULTIDITHER ADAPTIVE ALGORITHMS

Hughes Research Laboratories

Sponsored By
Defense Advanced Research Projects Agency
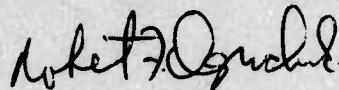ARPA Order No. 1279

DDC
RECEIVED
JUN 7 1976
A

ROME AIR DEVELOPMENT CENTER
AIR FORCE SYSTEMS COMMAND
GRIFFISS AIR FORCE BASE, NEW YORK 13441

This report has been reviewed by the RADC Information Office (OI) and is releasable to the National Technical Information Service (NTIS). At NTIS it will be releasable to the general public, including foreign nations.

This report has been reviewed and approved for publication.

APPROVED: *Robert F. Ogrodnik*

ROBERT F. OGRODNIK
Project Engineer

The views and conclusions contained in this document are those of the authors and should not be interpreted as necessarily representing the official policies, either expressed or implied, of the Defense Advanced Research Projects Agency or the U. S. Government.

Do not return this copy. Retain or destroy.

## REPORT DOCUMENTATION PAGE

READ INSTRUCTIONS
BEFORE COMPLETING FORM

| 1. REPORT NUMBER | 2. GOVT ACCESSION NO. | 3. RECIPIENT'S CATALOG NUMBER |
|---|---|---|
| RADC-TR-76-56 | | |

| 4. TITLE (and Subtitle) | 5. TYPE OF REPORT & PERIOD COVERED |
|---|---|
| MULTIDITHER ADAPTIVE ALGORITHMS. | Interim Report. 1 Aug — 31 Oct 75 |
| | 6. PERFORMING ORG. REPORT NUMBER |
| | N/A |

| 7. AUTHOR(s) | 8. CONTRACT OR GRANT NUMBER(s) |
|---|---|
| J. E. Pearson, M. L. Minden K. M. Brown, K. D. Price R. G. Finucane, G. Yeh | F30602-76-C-0022 ARPA Order - 1279 |

| 9. PERFORMING ORGANIZATION NAME AND ADDRESS | 10. PROGRAM ELEMENT, PROJECT, TASK AREA & WORK UNIT NUMBERS |
|---|---|
| Hughes Research Laboratories 3011 Malibu Canyon Road Malibu CA 90265 | 62301E 12790000 |

| 11. CONTROLLING OFFICE NAME AND ADDRESS | 12. REPORT DATE |
|---|---|
| Defense Advanced Research Projects Agency 1400 Wilson Blvd Arlington VA 22209 | April 076 |
| | 13. NUMBER OF PAGES |
| | 43 |

| 14. MONITORING AGENCY NAME & ADDRESS(if different from Controlling Office) | 15. SECURITY CLASS. (of this report) |
|---|---|
| Rome Air Development Center (OCTM) Griffiss AFB NY 13441 | UNCLASSIFIED |
| | 15a. DECLASSIFICATION/DOWNGRADING SCHEDULE N/A |

16. DISTRIBUTION STATEMENT (of this Report)

Approved for public release; distribution unlimited.

17. DISTRIBUTION STATEMENT (of the abstract entered in Block 20, if different from Report)

Same

18. SUPPLEMENTARY NOTES
RADC Project Engineer:
Robert F. Ogrodnik (OCTM)

19. KEY WORDS (Continue on reverse side if necessary and identify by block number)
COAT, Adaptive Optics, Thermal Blooming Compensation, Irradiance Tailoring,
Computer Simulation, Deformable Mirrors

20. ABSTRACT (Continue on reverse side if necessary and identify by block number)
Reduction of thermal blooming distortions has been studied as a function of
the initial transmitter irradiance profile. The data, obtained by computer
simulation of focused-beam propagation, indicate that the best way to increase
the peak target irradiance is to make the aperture distribution as uniform as
possible. This conclusion holds for Gaussian, truncated or apodized Gaussian,
annular or circular beams, and for special "hole-in-the-middle" laser modes.

Two computer simulations have been developed. One code calculates thermal

DD FORM 1473 EDITION OF 1 NOV 65 IS OBSOLETE

blooming correction with a full-servo simulation of a multi-dither COAT system. The second code models a multidither Zernike-polynomial COAT system (ZEP-COAT) with up to 13 polynomials. This code can be used with or without a simulation of a 37-element deformable mirror. Identical performance is obtained for linear propagation with the ZEP-COAT code and with a conventional multidither, outgoing-wave COAT (MOW-COAT) simulation code.

A 37-element deformable mirror has been designed for use with the DARPA/RADC 18-channel, visible-wavelength multidither COAT system. The design and performance goals of this uncooled mirror are summarized.

# PREFACE

This report was prepared by Hughes Research Laboratories, Malibu, California under contract F30602-76-C-0022. It describes work performed from 1 August 1975 to 31 October 1975, the first contract quarter. The principal investigator and principal scientist is Dr. James E. Pearson. The project is part of the adaptive optics program in the Opto-Electronics Department, managed by Dr. Viktor Evtuhov, at Hughes Research Laboratories.

# SUMMARY

The objective of this program on coherent optical adaptive techniques (COAT) is to investigate algorithms and techniques that can reduce the beam distortions caused by thermal blooming. This report covers the first contract quarter, from 1 August 1975 through 31 October 1975. The work during this quarter has centered on the design of a deformable mirror and on computer simulation studies.

The design and preliminary performance analysis of a 37-element, all-beryllium deformable mirror has been completed. The mirror will be used with the DARPA/RADC COAT electronics in experimental studies of thermal blooming compensation. The unit has drivers made of stacks of piezoelectric (PZT) washers and can be employed without additional electronics with the DARPA/RADC COAT system. The mirror will provide ±0.5 μm of surface motion (±2λ phase shift at 0.48 μm) with ±125 V of drive. The entire structure is uncooled. The analysis indicates that the lowest structural resonance will occur between 12 kHz and 15 kHz and the next resonance will be near 25 kHz. The analysis provides no information on the expected Q of these resonances. The PZT actuators themselves have no resonances below 40 kHz. The mirror is now under construction.

We have completed the modifications to our computer simulation of Zernike polynomial COAT (ZEP-COAT). This type of COAT system dithers and corrects on the coefficients of selected Zernike polynomials (focus, tilt, astigmatism, etc.) rather than on individual regions of the wavefront of a transmitted beam. The code at present can handel the first 13 Zernike polynomials with or with the added complexity of a full deformable mirror simulation.

We are utilizing a technique developed on the Hughes IR&D program for simulating multidither COAT compensation for thermal blooming. The technique greatly reduces the computer cost of such simulations and is exact for point receivers and single-glint targets.

This program will be used for all the multidither and ZEP-COAT computer studies on this program.

We have investigated by computer simulation the magnitude of thermal blooming distortions for different transmitter intensity profiles. We have so far found that the best way to reduce the blooming distortions, and thus to increase the peak focal-plane beam irradiance, is to make the initial intensity distribution as uniform as possible. This conclusion is true for Gaussian, truncated or apodized Gaussian, annular or circular beams, and for special "hole-in-the-middle" laser modules.

Plans for the second quarter include completion of the mirror construction and construction of the electronic Zernike-polynomial "generator" required to implement ZEP-COAT with the DARPA/RADC COAT electronics and the 37-element deformable mirror. We will also build a dither-injection unit that will apply both dither and correction signals to the deformable mirror used in a conventional multidither COAT system. Computer simulation studies will include ZEP-COAT blooming compensation and further intensity-tailoring investigations. An analysis of the convergence properties of a ZEP-COAT system will be started.

# TABLE OF CONTENTS

SECTION

# LIST OF ILLUSTRATIONS

# I. INTRODUCTION

## A. Program Objectives

The primary objective of this program on coherent optical adaptive techniques (COAT) is to analyze and experimentally demonstrate adaptive multidither correction algorithms that can reduce beam distortions caused by thermal blooming. The use of fixed transmitter intensity profiles for reducing thermal blooming will also be investigated.

## B. Research Program Plan

The research program utilizes the 21-channel DARPA/RADC experimental COAT system built and tested on contracts F30602-73-C-0248 and F30602-75-C-0001. Computer simulation codes developed on these contracts and on other programs (e.g., NSWC contract N60921-74-C-0249) will be used for the analytical portions of this contract. These codes model the operation of several types of COAT servomechanisms as well as the time-dependent propagation of optical beams in an absorbing and turbulent medium. The experimental investigations require construction of a deformable mirror for the COAT system as part of the program.

To accomplish the objectives of this contract, a 12-month research program consisting of three major tasks was developed. The program schedule, shown in Fig. 1, runs from August 1, 1975 through July 31, 1976. The analytical task dominates the first quarter of the contract. The design of the deformable mirror and initiation of its construction is also accomplished during the first quarter. The last half of the program is devoted exclusively to experimental studies of thermal blooming compensation with Zernike-Polynomial COAT (ZEP-COAT) and multidither outgoing-wave COAT (MOW-COAT).

4602-1

| 1975 | | | | | | 1976 | | | | | | |
|---|---|---|---|---|---|---|---|---|---|---|---|---|
| A | S | O | N | D | J | F | M | A | M | J | J |

Task 1

Task 2

← Analytical Studies →

Experimental Studies →

- Simulation Mod's
- Intensity tailoring
- ZEP-COAT Analysis

← Construction of ZEP-COAT Hardware →

← Thermal Blooming compensation with ZEP-COAT and MOW-COAT →

Task 3

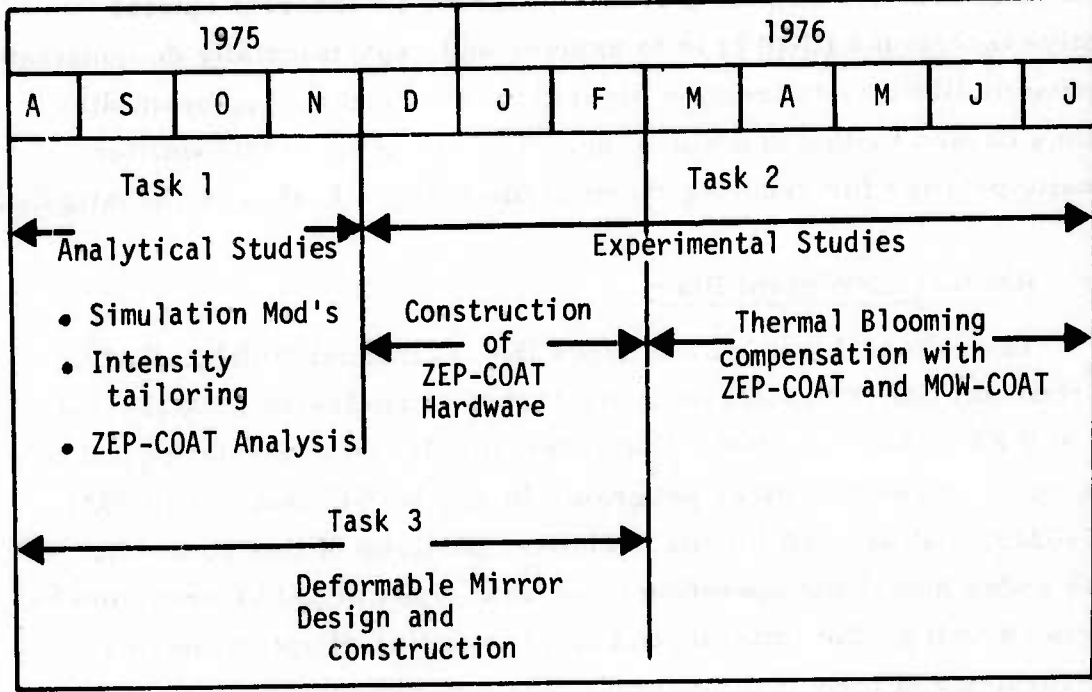← Deformable Mirror Design and construction →

Figure 1.   Research program schedule for Multidither Adaptive Algorithms studies.

## II. TECHNICAL ACCOMPLISHMENTS

During the first contract quarter, we completed the design and analysis of the deformable mirror that will be used with the DARPA/ RADC COAT system electronics to implement a Zernike-Polynomial COAT system (ZEP-COAT). Construction of the mirror was started during the quarter. The bulk of the analytical work on the contract was also accomplished. The following sections detail these accomplishments.

### A. Deformable Mirror Design and Construction

#### 1. Mirror Performance Goals

The mirror being built on this contract will replace the beam-splitter/phase-shifter array (called the "phasor matrix") that has been successfully used up to now with the DARPA/RADC COAT system.[1-5] It will perform the two functions of phase dithering (tagging) and phase correction required in any type of multidither COAT system. Performance of both these functions with a single element places heavy and conflicting demands on the device. The phase correction function requires large amplitude phase excursions (about ±2 optical wavelengths) at relatively low frequencies (up to about 1 kHz). On the other hand, the dither function requires low amplitude excursions (±30°) at much higher frequencies (10 to 30 kHz). To date, no continuous-surface, deformable mirror device has ever been constructed that can accomplish both of these functions simultaneously, particularly with the low drive voltages (±125 V) available from the DARPA/RADC COAT system.

The mirror being built on this program is the first of a kind and as such will represent the state of the art for uncooled deformable mirrors of its type. Because such a mirror had not been built, or event designed previously, an extensive design effort was initiated. This design has been funded only in part by this contract, the remainder of the work being performed as part of the Hughes Aircraft IR&D program.

The design and analysis effort started with Hughes-proprietary designs for a multielement deformable mirror and for external-spring, self-contained piezoelectrically-driven actuator cells. The performance goals of the design are listed in Table 1. The number of actuators was set by a compromise between available funds and the number of actuators required to produce the first 7 to 10 Zernike polynomials (see Section II-B-2). Beryllium was chosen as the structural material because of its large stiffness-to-weight ratio and reasonably low thermal expansion coefficient compared to molybdenum or aluminum. The structural resonant frequencies should be about $\sqrt{6}$ higher when using beryllium instead of molybdenum in a given design.

Table 1. RADC Deformable Mirror Performance Goals

| | |
|---|---|
| Faceplate excursion | ±0.5 μm (±2 phase shift at λ = 0.488 μm) with ±125 V of drive |
| Surface flatness | λ/2 overall; λ/6 over any localized actuator area |
| Frequency response | In excess of 10 kHz, but as high as possible |
| Structural material | Beryllium |
| Piezoelectric material | Gulton 6-1512 |
| Number of actuators | 37 in a circular arrangement |
| Mirror surface | Solid, uncooled |
| Actuator cooling | Not required for visible wavelength operation |

T1795

## 2. Mirror Design

A schematic of the mirror is shown in Fig. 2. The entire mirror body is made of beryllium. The 37 actuators are placed on a circular array with a minimum actuator spacing of 0.550 in. The active mirror surface has a diameter of 3.980 in. The faceplate is initially 0.055 to 0.060 beryllium stock, and is butt brazed to each of the 37 actuators and to the rim of the primary backup. The faceplate will be polished and coated with protected silver. The actuator cells are brazed to the primary backup at the same time as the faceplate braze. A braze test is currently in progress to establish the viability of the brazing techniques and the strength of the bonds before committing the entire struc-ture to the brazing process. The brazing techniques are similar to those that have been successfully used on other Hughes-built mirrors made of molybdenum, but the differences between molybdenum and beryllium braz-ing make the preliminary test a necessity.

Each mirror actuator is composed of a cylindrical spring assembly which houses a stack of 19 piezoelectric annular washers. A schematic of a single cell is shown in Fig. 5. Each washer is 0.024 in. thick, made of Gulton 6-1512 material. The cell is attached to the backup structure so that its entire length is effective in producing surface motion.

The transducer stack is electrically grounded at the mirror faceplate and the driver voltage is applied through the electrode at the other end of the PZT stack. With this arrangement, the transducer stack is internally wired, thus eliminating the complication of feeding wires out from the stack. The only wire to each actuator is conveniently soldered to the elec-trode in a manner which directs the wire straight out of the cell, with no bends requiring additional volume. This electrical arrangement is compati-ble with the electronics of the DARPA/RADC electroncis, which has a

4882-3

ELECTRICAL CONNECTION

PRELOAD SCREW

ACTUATOR CELL

PZT STACK

MIRROR FACE
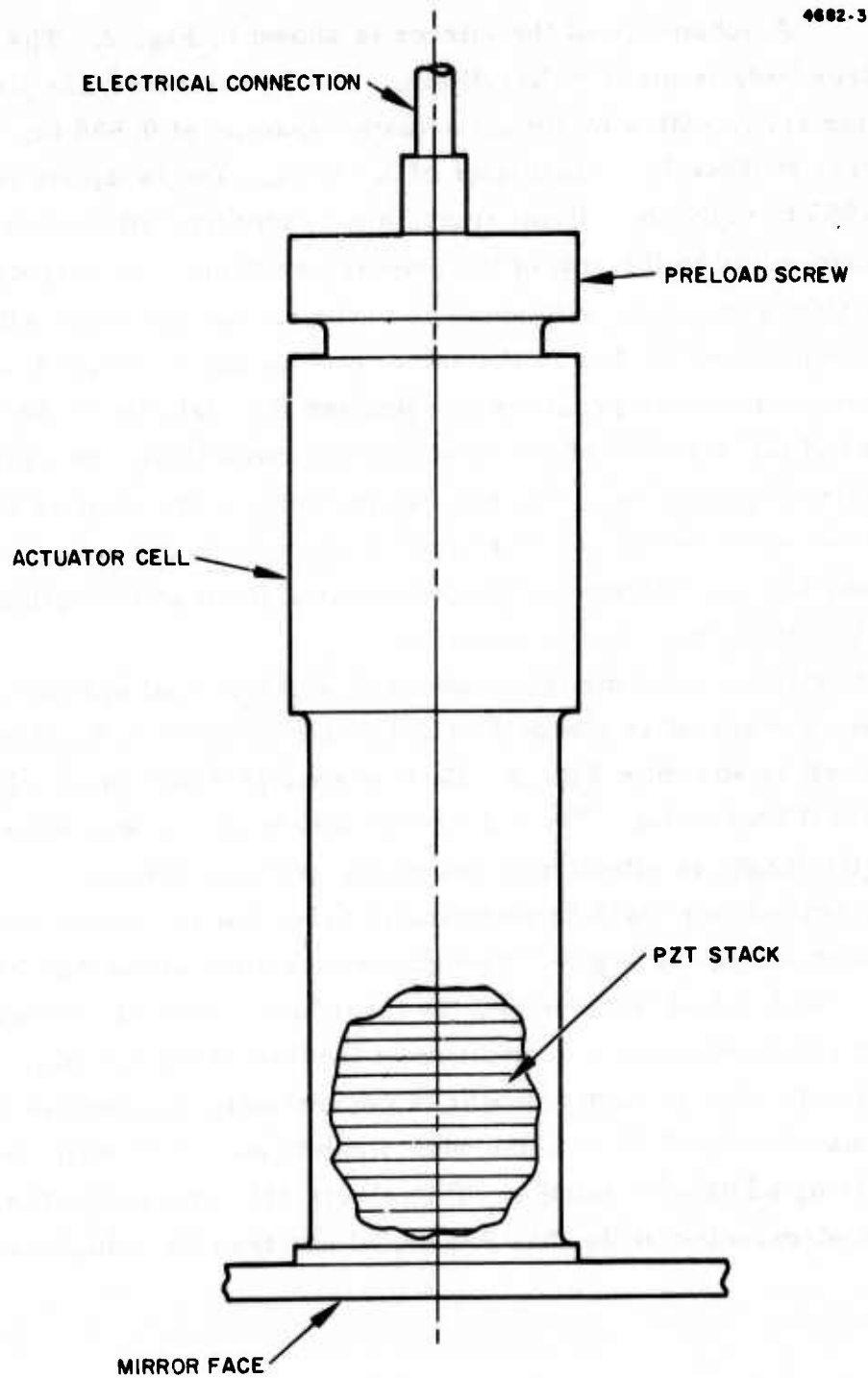
Figure 2. Schematic of 37-actuator deformable mirror
designed and now under construction on this
contract.

4682-4

EXTERNAL
MOUNT POINTS

SEALED REAR
DUST COVER

4I-PIN ELECTRICAL
CONNECTOR

3.50

1.30

4.380
DIA

ACTUATOR LOCATIONS
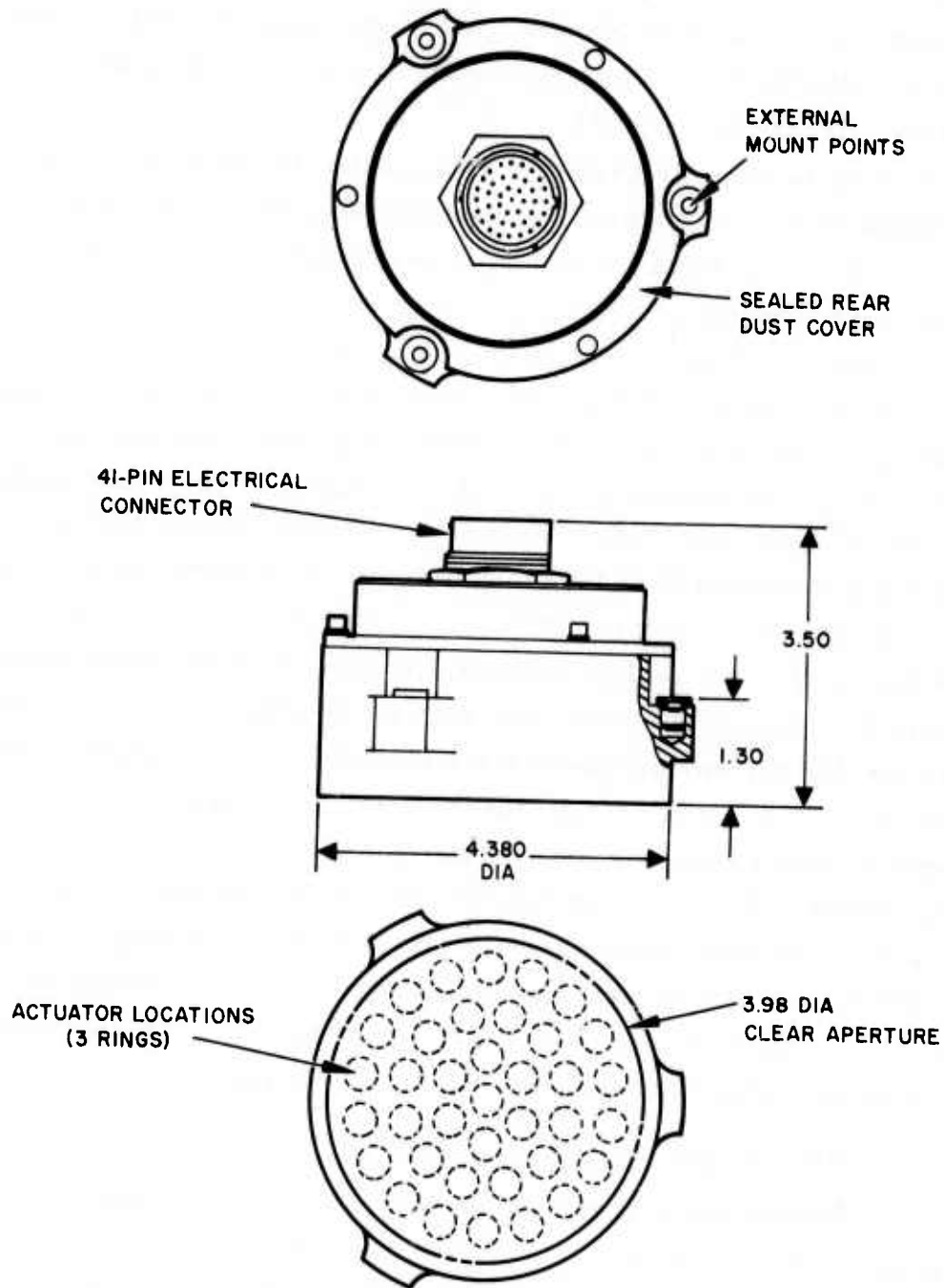(3 RINGS)

3.98 DIA
CLEAR APERTURE

Figure 3. Schematic of a single PZT actuator cell in the DARPA/RADC deformable mirror. All dimensions are in inches.

common ground for all channel outputs. All of the electrical outputs are brou_ht to a 41-pin electrical connector that is attached to the dust cover at the back of the mirror (see Fig. 2).

Each stack is to be preloaded to a nominal value of 32 lb. This is accomplished by torquing a preload screw to 30 to 35 in.-oz. The preload screw bears against an antirotation washer so that torque is not transmitted to the transducer.

The estimated weight of the mirror is 2.20 lb. The active portion of the mirror weighs 1.75 lb. (The mass of the cover and electrical feedthrough is not considered active.) Since the primary backup supports the actuators and faceplate, and weighs about 1.14 lb, structurally dead mass constitutes about 35% of the mirror. Initial design concepts sought to employ a reactionless type mounting for the actuator cell. The purpose of this type of mounting was to reduce or eliminate coupling of the transducer forces into the backup strcture. However, subsequent analysis revealed that the effect of the additional dead mass required in a reactionless design for this mirror produced more detrimental effects than did the transducer forces. The analysis discussed below indicates that due to the large amount of dead mass, the lowest resonance of the mirror will be about 12 to 15 kHz. This is lower than the 18.2 kHz first natural frequency reported earlier, because more recent analysis indicates a larger actuator spacing would be required in order to limit actuator cross coupling to below 5%. This larger spacing also allows for a thicker faceplate to be used so that interactuator bowing problems will be reduced.

3.    Mirror Performance Analysis

Considerable attention has been given to analyzing the frequency response of the mirror. The actuator cell/transducer assembly has been analyzed by two independent techniques — one using a distributed mass model, and one using a lumped mass model. Both techniques indicate a first natural frequency of about 50 kHz for the loaded actuator.

A finite-element model of the mirror was formulated using the Stardyne structural analysis program. A modal analysis of this model

gives the natural frequencies and associated mode shapes, but does not provide estimates of the resonance Q values. When the actuators are put into this model of the total mirror structure, the overall structure has a lowest resonance frequency of about 12 to 15 kHz. This mode appears to be a shear mode of the backplate structure.

Above the first resonance, the mode structure of the mirror becomes quite complicated and difficult to analyze. The analysis indicates that the next one or possibly two resonances with be below 25 kHz. Although these frequencies are within the 8-to 32 kHz dither band presently employed in the DARPA/RADC COAT system, and appropriate distribution of actuator frequencies on the circular area will minimize modal excitation, as will judicious selection of the dither frequencies to avoid the resonances. This will be accomplished by locating the actuators which must operate at frequencies near structurel resonances at the nodal points in the structure for these resonances.

Even with these low frequency resonances, however, there is some evidence that the COAT system performance will not be degraded. First, since the resonance modes are in the backup structure, there will be no loss in amplitude response of the actuators between the resonances. The primary loss in amplitude response will not occur until drive frequencies exceed the 50 kHz resonance of the PZT actuator assemblies. Second, we have had the opportunity to test a 37-element deformable mirror with this COAT system. The mirror, a cooled-faceplate unit built for NRL, had a low-Q first resonance around 4 kHz. In the tests, the dither frequencies were not applied to this mirror, but rather were put on the beam with the present beamsplitter phasor matrix assembly. The convergence time of the system with the NRL mirror as the corrector element was 1.5 msec and the system operation was stable. In short, the performance was equal to that observed previously with the COAT system using the phasor matrix for both dither and corrector functions.

A second area of investigation has been the response of the mirror body to unbalanced actuator excitation. The amplitude of response of the mirror backup is proportional to the magnitude of the unbalanced forces in the actuators. For a beryllium structure, the unbalanced forces are due almost entirely from the relatively massive PZT stacks. This

19

force can be calculated by using

$$F_{RMS} = \pi^2 \sqrt{2} \frac{w}{g} uf^2 \qquad (1)$$

where w is the weight of PZT stack and cell, g is the acceleration of gravity, u is the maximum excursion of mirror, and f is the driving frequency.

A 1/4 in. diameter actuator weighs about 0.010 lb, and the required dither motion is about ±2 μin. The RMS force is therefore

$$F_{RMS} \approx 7.2 \times 10^{-10} f^2 \text{ lb.}$$

At 15 kHz, the force is 0.163 lb. Assuming an amplification factor (Q) of 15 for the beryllium mirror at the 15 kHz resonance, and a limit of 0.2 μin. due to structural vibrational motion, the mirror must have a stiffness of at least

$$K = \frac{QF}{u} = \frac{(15)(0.146)}{(0.2 \times 10^{-6})} \text{ lb/in} = 12 \times 10^6 \text{ lb/in.}$$

Our analysis indicates that the stiffness of the mirror (referenced to a load at the center actuator) is of the order of magnitude $10^7$ lb/in. Since the actuators will not be driven at or near natural frequencies, we do not expect that mirror performance will be degraded by unbalanced actuators.

The final major design consideration was the tradeoff among faceplate thickness, resonant frequencies, mirror motion, and number

of PZT washers in each actuator cell. The motion, u, of the mirror surface may be described by

$$K_A \geq \frac{\dfrac{K_B}{\eta \delta_F}}{\dfrac{\delta_F}{u} - 1} \qquad (2)$$

$$\eta \geq \frac{u}{\delta_F} \frac{(K_A^{-1} + K_B^{-1})}{K_B^{-1}} \qquad (3)$$

$$K_A^{-1} = K_P^{-1} + (\eta+1)K_e^{-1} + K_s^{-1} \qquad (4)$$

where

$K_A$ ≡ Transducer assembly stiffness (lb/in)

$K_B$ ≡ Actuator cell plus faceplate stiffness (lb/in)

$\eta$ ≡ Number of active PZT washers

$\delta_F$ ≡ Free expansion of one PZT washer (in)

  $= d_{33} \Delta V$

$d_{33}$ ≡ Piezoelectric charge coefficient (in/volt)

$\Delta V$ ≡ Applied voltage (volts)

u ≡ Motion of mirror surface (in)

$K_P$ ≡ Stiffness of one PZT washer

$K_e$ ≡ Stiffness of one electrode

$K_s$ ≡ Total stiffness of all remaining elements in transducer stack.

Since in most mirror applications u is defined, equations (2) to (4) can be rearranged into a more useful form to give the minimum required number of washers, $\eta$:

$$\eta \geq \frac{u/\delta_F \left(K_B^{-1} + K_e^{-1} + K_s^{-1}\right)}{K_B^{-1} - u/\delta_F \left(K_P^{-1} = K_e^{-1}\right)} \tag{5}$$

Equation 5 has been solved parameterically for a number of PZT dimensions and materials. The final design values chosen are listed in Table 2.

At the present time, most of the mirror components are being fabricated, either by Hughes or by outside vendors. No difficulties have arisen regarding fabrication and assembly, and delivery for test with the COAT system is scheduled on or before 1 March 1976.

## B.     Analysis

Most of the analysis that will be performed on this contract has been completed during this quarter. The mirror analysis has already been described. This section describes the computer simulation work that has been accomplished on Zernike-polynomial COAT (ZEP-COAT) and on transmitter intensity tailoring for reducing thermal blooming.

### 1.     Computer Simulation Modifications

a.     Thermal Blooming — As part of the previous RADC/COAT contract (No. F30602-75-C-0001), we had planned to use computer simulation to study thermal blooming compensation with a multidither COAT system. To our dismay, however, we found that the existing propagation code and multidither servo code could not be operated together without prohibitively long computer run times. Consequently, we obtained no simulation data for multidither blooming compensation.

Table 2. Final Design Values used in Calculations

| | | |
|---|---|---|
| $\eta$ | 29 | |
| $K_B$ | $0.9 \times 10^6$ lb/in. | |
| $K_{cell}$ | $0.7 \times 10^6$ lb/in. | |
| $K_{faceplate}$ | $0.2 \times 10^6$ lb/in. | |
| $K_e$ | $8.0 \times 10^8$ lb/in. | |
| $K_s$ | $10^7$ lb/in. | |
| PZT Washer: | | |
| Outside Diameter | 0.255 | 0.005 |
| Thickness | 0.0235 | 0.001 |
| Material | G-1512 | |

Shortly after the end of the previous contract, we conceived of a new numerical technique which will allow the multidither simulation work to proceed. The approach is valid only for a single "point-glint," but this restriction is not an important limitation for the purposes of this contract.

To summarize this approach briefly, we have shown that the field at a target point in the presence of turbulence and thermal blooming can be calculated from a Green's function, calculated numerically by running the propagation code backwards with a point source at the point of interest. Although this is a rather obvious result in theory, it is not obvious that this can be done numerically because the propagation code does not handle point source fields very well because of problems caused by large angle scattering interacting with the edge of the mesh. We have shown, however, that the errors caused by these edge effects apparently cancel when the point source function, i.e., the Green's function, is multiplied by the initial wave to obtain the field at the point in question.

This technique for evaluating the field at a point will allow us to simulate the operation of multidither COAT systems in the presence of turbulence and thermal blooming without having to run the full scale propagation code every dither cycle. For example, if it is assumed that there is a point receiver located at the target, we can simply run the propagation code backwards once to determine the Green's function and then use this Green's function to evaluate the field at the receiver over a number of dither cycles. We must, of course, eventually update the Green's function to account for changes in the properties of the medium induced by local winds and heating, but this update time is typically much larger than the multidither servo system time increment ($\sim 5$ $\mu$sec for a 37-channel COAT system with a 1 ms response time).

We have also shown that the same type of approach can be used in a multidither simulation in which there is a point receiver located in or near the transmitter aperture.

b.     ZEP-COAT — There are two principal multidither adaptive algorithms that will be explored on this contract: (1) multidither, outgoing-wave COAT (MOW-COAT), and (2) Zernike-polynomial COAT (ZEP-COAT). The MOW-COAT algorithm is also referred to as "zonal-COAT," since each separate region or "zone" in the transmitted wave-front is dithered and corrected independently of the rest of the wavefront. This is the type of system that has been employed in all of our work to date.[1,8] In ZEP-COAT, however, the entire wavefront is acted upon by each dither/correction channel. Instead of acting upon isolated regions of the wavefront, a ZEP-COAT system adjusts the amplitudes of the coefficients, $\beta_n$, in the expansion

$$\phi_T = \sum_{n=1}^{N} \beta_n Z_n (r, \theta) \quad , \tag{5}$$

where $\phi_T$ is the transmitted beam phase front, $Z_n (r, \theta)$ is the $n^{th}$ Zernike polynomial,[9] and $(r, \theta)$ are the polar coordinates at the transmitter. The correction phasefront is impressed on the transmitted beam using a deformable mirror. Each ZEP-COAT servo channel produces one coefficient in the expansion in Eq. (5) and thus influences the entire wavefront, not just one region of it.

The equivalence of ZEP-COAT and MOW-COAT is reasonably obvious for linear propagation, since in each system the servo acts to produce the $\phi_T$ that maximizes the target irradiance. In fact, any function set that is orthogonal over the transmitter aperture could be used in the expansion for $\phi_T$; the individual "zones" and Zernike poly-nomials are only two choices. The Zernike polynomials are a par-ticularly convenient choice since they are also used to represent the classical abberations[9,10] and have been used by others[11] in blooming compensation studies. Our goal in studying ZEP-COAT is to develop a COAT system which can compensate for thermal blooming as effectively as, or hopefully better than, a zonal MOW-COAT system, and use fewer servo channels to accomplish the correction.

The computer simulation of the ZEP-COAT system has been broken into two programs to minimize computer run time and thus costs. The first program is a modification of the HRL MDDTB (Multi-Dither, Deformable Mirror, Thermal Blooming) computer code described previously. The MDDTB code models corrections for both turbulence and pulsed thermal blooming using a deformable mirror. The response of the mirror to the servo output is calculated every 40 µsec. The frequencies used to dither each actuator, however, require that the glint intensity be sampled every 5 µsec. Rather than recalculate the exact mirror surface every 5 µsec, MDDTB assumes the effect of each frequency dither to be confined to a local area surrounding its actuator, and constant over that area (in effect, a "piston" dither mirror).

The approximation used in MDDTB, which saves considerable computational time, is clearly not valid in any ZEP-COAT simulation. The ideal mirror surface would be described by

$$\phi_T(r, \theta) = \sum_n Z_n(r, \theta)(\beta_n(t) + \delta_n \cos \omega_n t), \qquad (6)$$

where the $Z_n$ are any of the Zernike polynomials listed[*] in Table 3, the $\beta_n$ are the deformation amplitude coefficients, and $\delta_n$ are the dither amplitude coefficients. The dither amplitude $\sum_n \delta_n Z_n(r, \theta)$ is neither localized nor constant about any point on the mirror, and the entire mirror profile must be recalculated at every time increment. If we add the stipulation that the ideal surface in Eq. (6) be produced by an actual deformable mirror, the additional calculations become extremely time consuming.

Thus, the first ZEP-COAT computer code, based on MDDTB, has removed the effect of the deformable mirror entirely and instead directly dithers the ideal Zernike surface (i.e., the coefficients in the expansion of Eq. (6)). The initial mirror deformation is set up by specifying

---

[*] Only the 13 lowest-order polynomials will be investigated on this contract; we expect that adding more will not significantly increase the blooming compensation observed.

Table 3. Zernike Polynomials Used in ZEP-COAT Simulation

| n | $Z_n$ | Aberration Name |
|---|---|---|
| 1 | $2R^2 - 1$ | Refocus |
| 2 | $6R^4 - 6R^2 + 1$ | Spherical aberration |
| 3 | $20R^6 - 30R^4 + 12R^2 - 1$ | 5th-order spherical aberration |
| 4 | $X$ | Horizontal tilt |
| 5[a] | $Y$ | Vertical tilt |
| 6 | $X(3R^2 - 2)$ | coma (Y-symmetry) |
| 7[a] | $Y(3R^2 - 2)$ | coma (X-symmetry) |
| 8 | $X(10R^4 - 12R^2 + 3)$ | 5th order coma (Y-symmetry) |
| 9[a] | $Y(10R^4 - 12R^2 + 3)$ | 5th order coma (X-symmetry) |
| 10 | $X^2 - Y^2$ | Astigmatism |
| 11 | $(X^2 - Y^2)(4R^2 - 3)$ | Astigmatism (5th order) |
| 12 | $X(X^2 - 3Y^2)$ | 120 degree (5th order, Y-symmetry) |
| 13[a] | $Y(Y^2 - 3X^2)$ | 120 degree (5th order, X-symmetry) |

where $X = \dfrac{x}{\sqrt{2}} = R\cos\theta$, $Y = \dfrac{y}{\sqrt{2}} = R\sin\theta$, and $R = x^2 + y^2 \leq 1$

[a] These four polynomials are not used for compensating only thermal blooming because of the symmetries in the blooming distortions (see Ref. 11). They are used for turbulence compensation.

T1796

starting values of the $\beta_n$. The medium is initialized by propagating several high power pulses through it to the single glint target to establish some level of thermal blooming (not a cw, or steady-state medium, however). The COAT system is then turned on for a fraction (about 1/5) of a free-space convergence time (about 1 msec).

Every 5 $\mu$sec the new correction phase resulting from dithering is calculated, and the beam is propagated linearly through the fixed medium. The propagation calculations in this program are implemented by weighting the transmitted complex field by a Green's function (determined from the medium characteristics and glint position) as explained above, and by taking a sum over a grid of 25 x 25 points. The resulting glint intensity signal is processed by the COAT servo which, after 40 $\mu$sec, returns updated values for the $\beta_n$. In about 0.2 msec, the beam shape has changed sufficiently to require redetermination of the thermally-bloomed medium. Typical runs made so far last a total of 2 msec, or 10 medium updates (10 pulses). This is not enough to reach a good medium steady state,[12] however, and longer runs will be required in the future.

The second program is a modification of the HRL code CMDDM (Coherent-Multidither, Deformable Mirror). This code, developed as part of the HICLAS program (NSWC contract No. N60971-76-C-0008), treats only turbulence and consequently requires far less time. For this reason, it was decided to use the deformable mirror model here for our early tests, and to incorporate the model into the thermal blooming code only if the modelled mirror appears to significantly affect the ZEP-COAT performance results.

The ZEP-COAT modification of CMDDM, like the original CMDDM and MDDTB codes, exactly calculates the low frequency mirror response and approximates the high frequency dither response. Determination of the low frequency response requires that the program

(1)     Use servo channel filter outputs, $\beta_n$, to evaluate
         the ideal surface deformation $\sum_n \beta_n(r, \theta)$ at the
         coordinates of each actuator

(2)     Use this ideal phase as the input signal to the
        actuator

(3)     Calculate the mirror surface from the new actuator
        positions.

As a first approximation, the dither perturbations were incorporated by adding the ideal dither $\sum_n \delta_n Z_n(r, \theta) \cos \omega_n t$ at each actuator point, and assuming the value to be constant over the area surrounding the actuator (effectively a "piston"-type dither). Eventually, the two programs may be combined into one so that the dithering is on the correct surface (the deformable surface). The results of the thermal blooming program, however, are interesting enough that mirror complications need not be added immediately.

## 2.     ZEP-COAT Studies

The test runs made with the ZEP-COAT code so far have included initial mirror deformations and the propagation of an initial set of high power pulses, followed by operation of the ZEP-COAT system with no medium updates. Figure 4 shows one of the simplest cases: correction of the system for initial mirror defocus, with no medium corrections (fixed initial medium). This performance is an improvement over that reported earlier.[8] No effort has yet been made, however, to optimize (minimize) the convergence time of the ZEP-COAT system.

In runs which modelled thermal blooming by updating the medium periodically, however, the ZEP-COAT system appears to become unstable after some unpredictable amount of time. Much of the effort in the next quarter will be put into an analysis of this instability to determine whether it is a fundamental effect or whether it is caused by a computer computational problem. One possible source of instability in a ZEP-COAT system which occurs with thermal blooming is the coupling of the polynomials by the nonlinear medium; the expansion set in Eq. (6) is no longer an orthogonal one. This "instability" behavior has not occurred for free-space propagation, or for linear turbulence and distortions, in any of our computer runs.
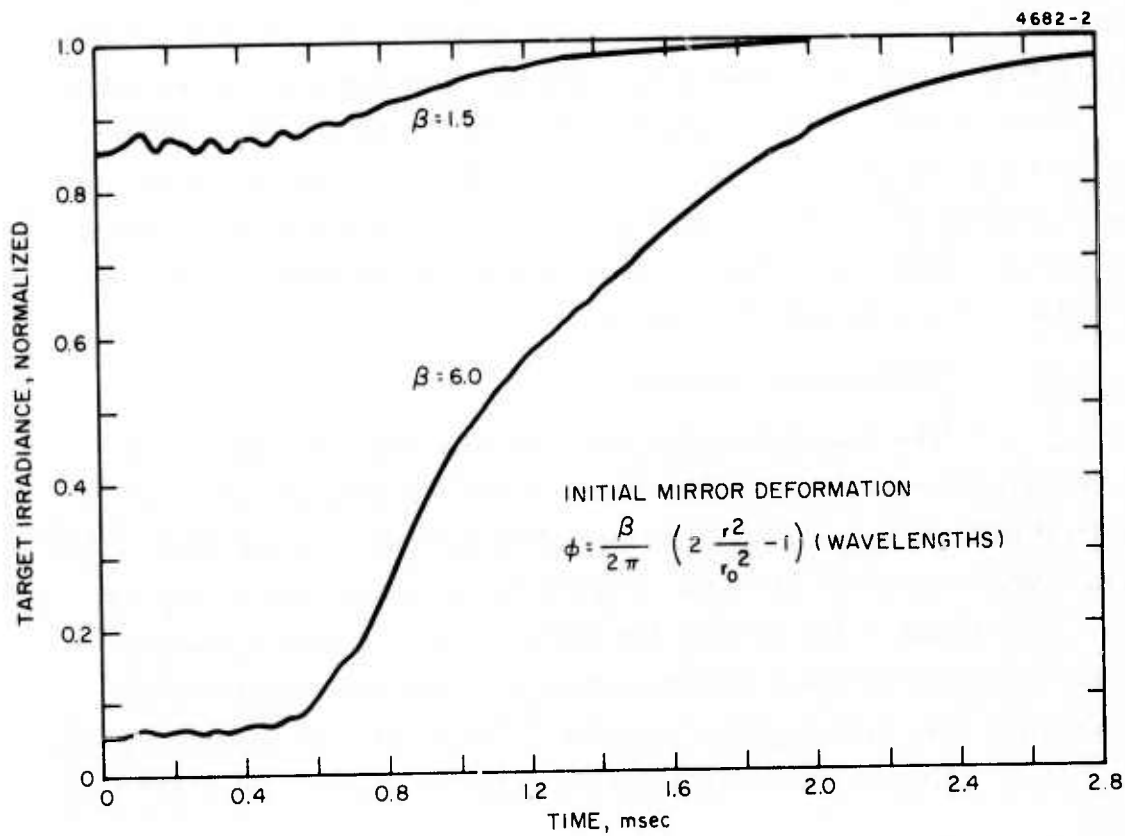
Figure 4.    Convergence of a nonoptimized ZEP-COAT system when the initial error is a simple refocus.

Our preliminary investigations have produced several results. First, the servo parameters do influence the instability behavior. The dither amplitude has a strong effect on the length of time the ZFP-COAT system remains stable. Lowering the dither amplitude, and consequently the total servo loop gain, has not seemed to increase the stability. Controlling the gain of each channel separately has so far not yielded better results, although we are far from having done a careful optimization of the servo parameters.

Second, analytical problems arise when spatial components of the wavefront phase are no longer orthogonal to each other. The Zernike polynomials are initially orthogonal by definition, but the nonlinear propagation effects of thermal blooming will couple these modes together. An analysis is now underway to determine exactly what effect this might have on the error signals in each channel, and whether this could be serious enough to cause the instabilities. The analysis should also aid us in optimally setting the dither amplitude and the gain in each ZEP servo channel.

3.    Intensity Tailoring

The primary goal of this contract is to achieve a reduction of thermal blooming distortions and thus to maximize the peak irradiance that a focused beam can deliver to a target. Since some specific transmitter irradiance profiles have been shown[2,3] to be effective in reducing blooming, it was deemed appropriate that we should take a brief look at fixed transmitter irradiance profiles using our well-developed cw-blooming computer propagation code.

We have investigated several transmitter profiles that have an on-axis irradiance null. This investigation was initially motivated by the suggestion that the use of a transmitted beam that has an annular intensity profile may provide higher focal plane irradiance in the presence of thermal blooming[4] than that produced by a Gaussian beam. The physical reasoning behind this suggestion is straightforward. A Gaussian intensity profile produces a quadratic refractive index variation

in the medium that is minimum at the beam center where most of the optical power occurs. With an annular beam that has an on-axis null, the lens induced in the medium has a larger refractive index on-axis than off-axis. The result is a positive lens for light that is close to the beam axis, and this lens tends to counteract some of the off-axis negative-lens beam spreading as the optical beam propagates.

Two types of annular or "hole-in-the-middle" intensity profiles have been treated: (1) those that have an intensity zero in the beam center, both in the focal plane as well as at the transmitter and thus are free-space propagation modes; (2) those profiles that have a zero in the beam center only at the initial transmitter plane; due to diffraction, the initial on-axis null fills in as these beams propagate so that the on-axis irradiance is not zero at the focal plane. An appropriate choice of the initial profile can indeed increase the maximum target irradiance. The standard of comparison in all cases is the target irradiance produced by a Gaussian beam that is truncated at the 10% intensity radius.

We first consider cases where the intensity null in the middle of the beam is retained as the focused beam is propagated to the target. To first demonstrate than an appropriately chosen transmitter intensity distribution can indeed be focused to produce a "hole-in-the-middle" focal-plane irradiance distribution, we start with a transmitter aperture field given by[5]

$$A(r_1, \theta_1) = f_m(r_1) \cos (m\theta_1), \ (m + 0, 1, 2 \ldots), \tag{7}$$

where $f_m(r_1)$ may be a continuous or a discontinuous function of $r_1$ and $(r_1, \theta_1)$ are the transverse polar coordinates of the transmitting aperture. From Fresnel diffraction formulae, we obtain the field $u$ at the focal plane:

$$u(x_o, y_o, z) = \frac{e^{jkz}}{j\lambda z} \exp \left\{ j \frac{k}{2z} (x_o^2 + y_o^2) \right\} \cdot$$

$$\int\int_{-\infty}^{\infty} A(r_1, \theta_1) \exp \left\{ -j \frac{2\pi}{\lambda z} (x_o x_1 + y_o y_1) \right\} dx_1 dy_1 , \tag{8}$$

where $z$ is the ~~focal~~ local distance, $\lambda$ the free-space wavelength, $k = 2\pi/\lambda$, $(x_o, y_o)$ are the transverse rectangular coordinates at the target (focal) plane, and $(x_1, y_1)$ are the transverse rectangular coordinates at the transmitting aperture plane. Changing Eq. (8) into polar coordinates and carrying out the angular integration, we find

$$u(r_o, \theta_o, z) = \frac{e^{jkz}}{j\,z} \exp\left\{j\frac{k}{2z} r_o^2\right\} \int_0^\infty f_m(r_1) r_1 dr_1 \quad .$$

$$\int_0^{2\pi} \cos(m\theta) \exp\left\{-j\frac{2\pi}{\lambda z} r_1 r_o \cos(\theta_1 - \theta_o)\right\} d\theta_1 \quad (9)$$

$$= \frac{e^{jkz}}{j\lambda z} \exp\left\{j\frac{k}{2z} r_o^2\right\} 2\pi \cos(m\theta_o) e^{-j m\frac{\pi}{2}} I_m(r_o),$$

where

$$I_m(r_o) = \int_0^\infty f_m(r_1) J_m\left(\frac{2\pi}{\lambda z} r_1 r_o\right) r_1 dr_1, \text{ and} \quad (10)$$

$$\left|u(0, \theta_o, z)\right|^2 = \left[\frac{2\pi \cos(m\theta_o)}{\lambda z}\right]^2 I_m^2(0) \quad . \quad (11)$$

Since $J_m(0) = 0$ when $m = 0$, Eq. (10) indicates that $I_m = 0$ for $m = 0$. A hole-in-the-middle target irradiance is thus obtained for all $m = 0$. When $m \neq 0$, however, the on-axis target irradiance is never zero. Both of these conclusions are true independent of the initial radial dependent of u

Although the field example we have chosen (Eq. (7)) is a special case, the following conclusion is a general one: if the initial intensity distribution does not have an angular ($\theta_1$) dependence, the focal-plane irradiance cannot have an on-axis null. A particular example is the

"doughnut" mode formed by the Hermite-Gaussian modes,[6] $TEM_{10} + TEM_{01}^*$. The electric field of this combination mode has a $\theta$-dependence, but the intensity distribution has an on-axis zero and no $\theta$-dependence. The far-field intensity pattern of this mode combination does not have an on-axis null.

The particular transmitter intensity profiles that we have chosen to study are given in Eqs. (12) and (13) and are illustrated in Fig. 5. The truncated Gaussian beam we are using for comparison purposes is also shown in Fig. 4 and defined in Eq. (14).

Case
(II-a)
$$|u|^2 = e^{-r_1^2/\rho_o^2} \sin^2\theta_1, \text{ for } r_1 \leq a_o \tag{12}$$
$$= 0, \qquad\qquad\qquad \text{for } r_1 > a_o$$

Case
(II-b)
$$|u|^2 = e^{\left(\frac{r_1-r_m}{\rho_o}\right)^2} \rho^2 \sin^2\theta_1, \text{ for}$$
$$b_o \leq r_1 \leq a_o \text{ and } b_o < r_m < a_o \tag{13}$$
$$= 0, \text{ otherwise}$$

Truncated
Gaussian
$$|a|^2 = e^{-r_1^2/\rho_o^2}, \text{ for } r_1 \leq a_o \tag{14}$$
$$= 0, \quad \text{otherwise} \quad .$$

For these beams, the first two of which can be produced by coaxial-resonator, annular-gain lasers,[5] $\rho_o$ is the e-folding intensity radius of the Gaussian beam in Eq. (8), $\rho$ is a constant less than or equal to 1, $r_m$ is the adjustable maximum-intensity radius, and $b_o$ and $a_o$ are the inner and outer radii of a coaxial laser resonator. The beams in
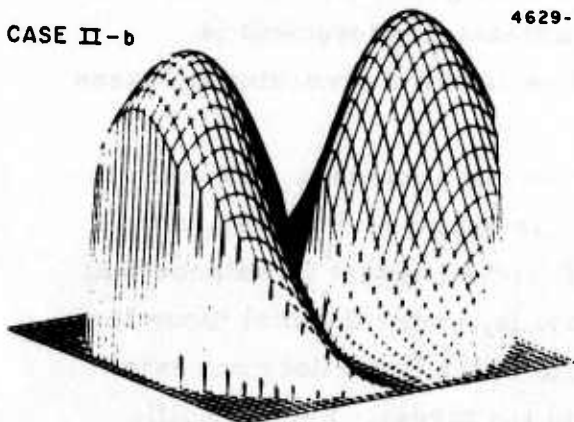
4629-9
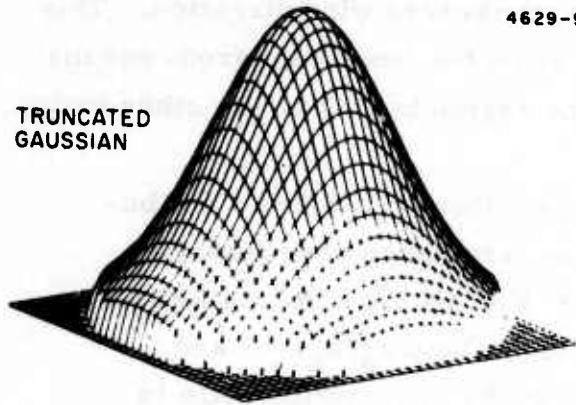
TRUNCATED
GAUSSIAN

4629-8
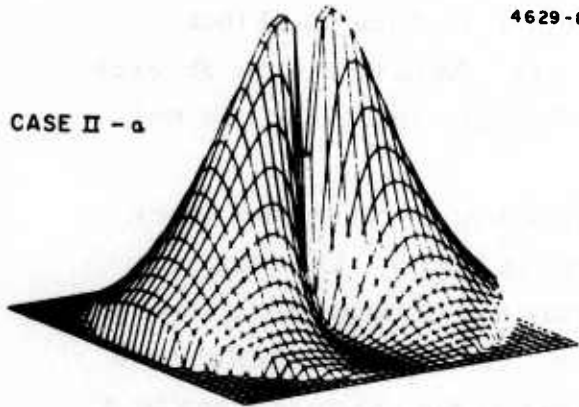
CASE II – a

4629-7

CASE II – b

Figure 5.
Three-dimensional plots of transmitter irradiance profiles that retain their shape as they propagate. The truncated Gaussian beam is used as a comparison reference for all other beams considered. The two "hole-in-the-middle" profiles shown here also have an on-axis null in the focal plane.

The beams described by Eqs. (12) and (13) are assumed oriented in such a way that the $\theta_1 = 0$ axis is parallel to the transverse wind direction. This orientation produces minimum blooming since the heated air from one main transmitter lobe does not pass through the region heated by the other main lobe.

Figure 6 compares the initial transmitter irradiance distributions of the three beams to the focal-plane irradiance distributions for a representative transmitter power.* For all the computational results presented here, we have chosen the values $a_o/b_o = 7$ and $\rho = 1$. The choice of $a_o/b_o$ corresponds to the obscuration ratio in some laser pointer/tracker systems now in use. The value $\rho = 1$ gives the most uniform initial intensity distribution; we have found that thermal blooming is minimized for this case. Note that in the absence of blooming effects, the focal plane distributions would look like the transmitter distributions for each case.

The peak target irradiance as a function of transmitted laser power for these three beam cases is given in Fig. 7. The maximum target irradiance for Case (II-b) is a factor of 1.2 larger than that obtained with the truncated Gaussian beam. The higher irradiance is obtained by increasing the total laser power at the aperture plane by a factor of 1.3. Case (II-a) yields lower peak target irradiance even with higher total laser power. Hence, no significant improvement is obtained with transmitting intensity profiles tailored according to Cases (II-a) or (II-b).

We now treat cases for which the on-axis intensity null will occur only at the transmitting aperture. As shown by Eq. (11), all angularly-independent annular beams will yield a target irradiance that has no on-axis intensity null. In other words, under thermal blooming conditions, the cooler region in the middle of the beam does not exist throughout the focused propagation path to the target. Four specific

---

*In these discussions, the laser power level is the total transmitted power. At a fixed laser power, the peak irradiance is thus different for each type of beam.
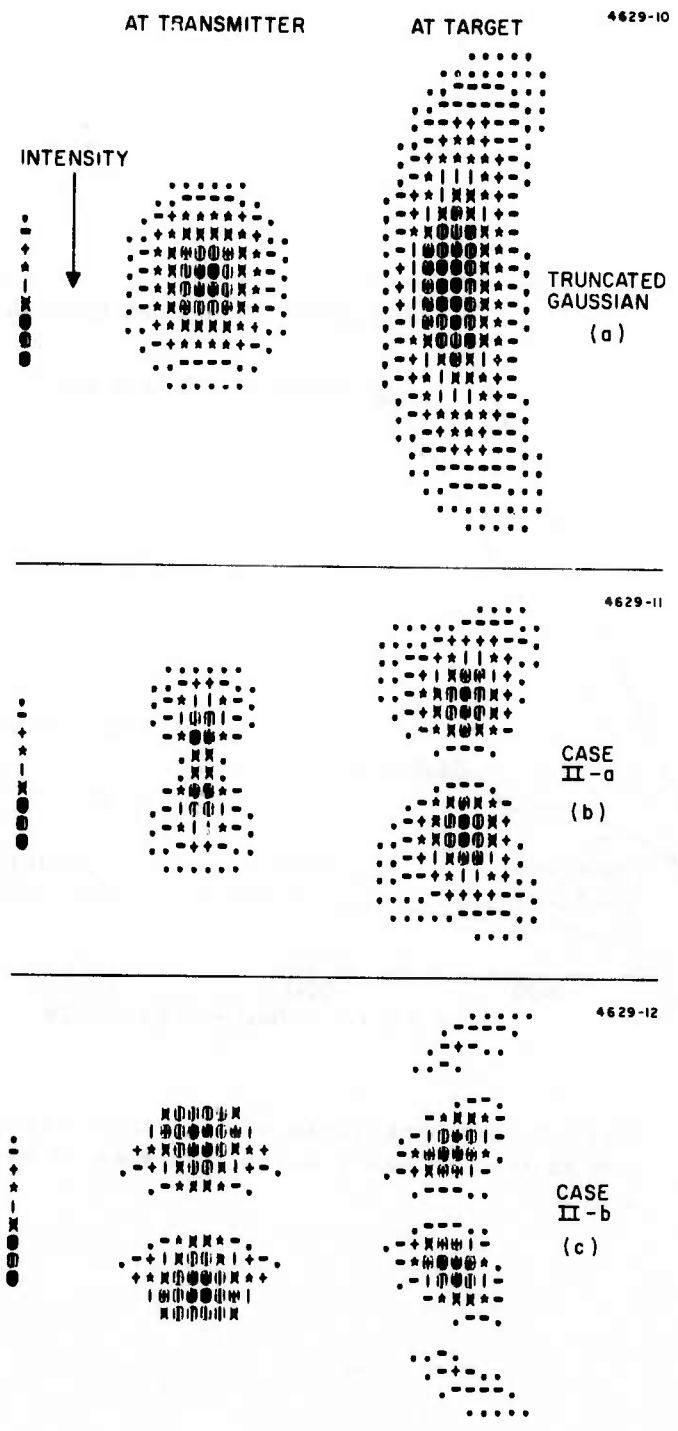
36

Figure 6.
Pseudo-gray sacle plots of transmitter and
focal-plane (target) irradiance distributions
for the three beams in Fig. 1. A moderate
amount of thermal blooming is present in
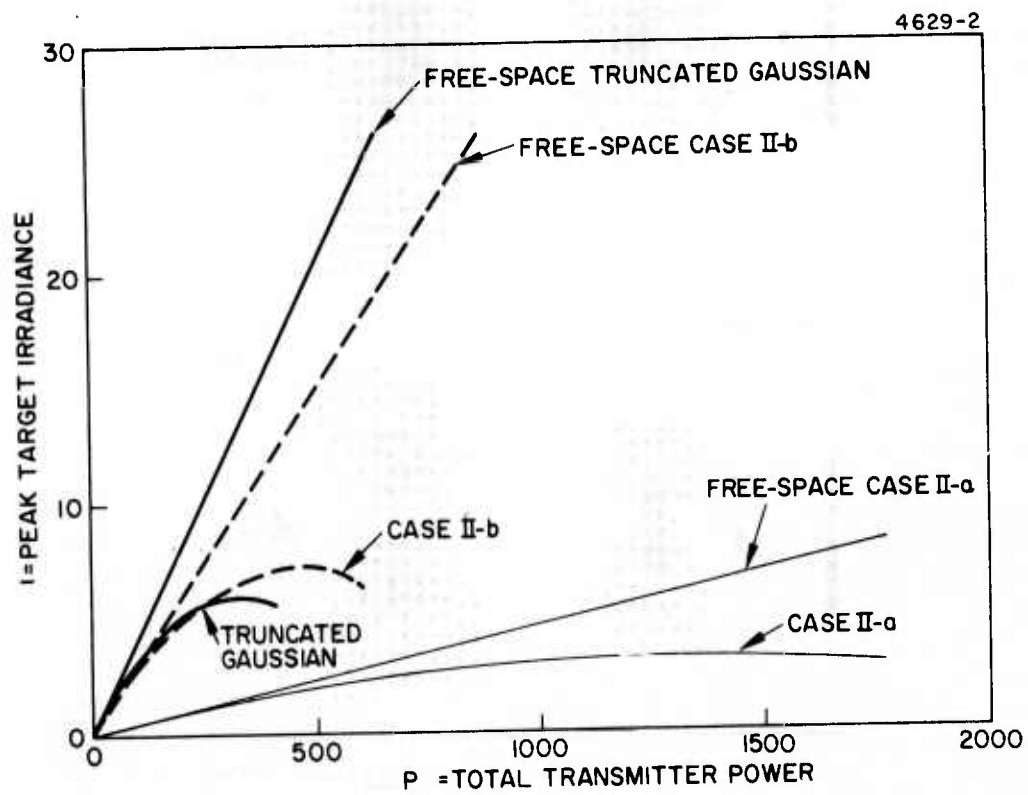the propagation path.

Figure 7. Peak target irradiance versus total transmitter power for the same three cases as in Figs. 1 and 2.

aperture intensity profiles are considered and compared to the truncated Gaussian in Eq. (8):

Case
(III-a)
$$u^2 = \left(\frac{r_1}{\rho_o}\right)^4 e^{-\frac{r_1^2}{\rho_o^2}} , \text{ for } r_1 < a_o \qquad (15)$$
$$= 0 \qquad\qquad , \text{ for } r_1 > a_o$$

Case
(III-b)
$$|u|^2 = e^{-\left(\frac{r-r_m}{\rho_o}\right)^2} \frac{1}{\rho^2} , \text{ for } b_o < r_1 < a_o \qquad (16)$$
$$= 0 \qquad\qquad , \text{ otherwise}$$

Case
(III-c)
$$|u|^2 = 1 \qquad\qquad , \text{ for } b_o < r_1 < a_o \qquad (17)$$
$$|u| = 0 \qquad\qquad , \text{ otherwise}$$

Case
(III-d)
$$|u|^2 = e^{-\frac{r_1^2}{\rho_o^2}} \qquad\qquad , \text{ for } b_o < r_1 < a_o \qquad (18)$$
$$= 0 \qquad\qquad\qquad \text{ otherwise}$$

Computer-generated plots of these beams are illustrated in Fig. 8.

The transmitter aperture intensity profiles as well as the corresponding target intensity profiles for these cases are displayed in Fig. 9 for a representative laser power level. Figure 10 compares the peak target irradiance as a function of total input transmitting power for these four cases to that for the truncated Gaussian case. Unlike the cases treated in Eqs. (12) to (14), significantly larger peak target irradiance is achieved for three of the four cases considered as compared with that for the truncated solid Gaussian. Only Case (III-d) yields a peak target irradiance which is below that for the truncated Gaussian beam.

CASE III-a
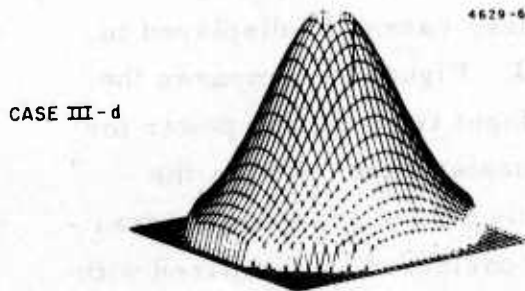
4629-3

CASE III-b

4629-4

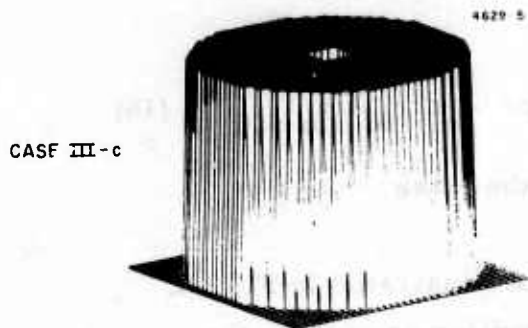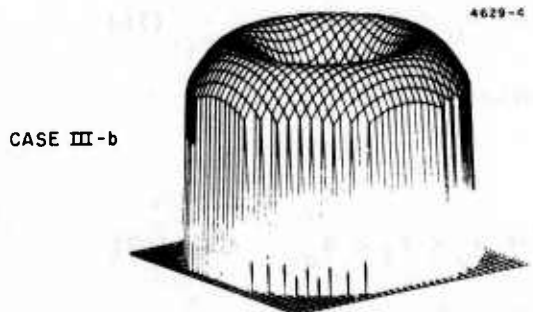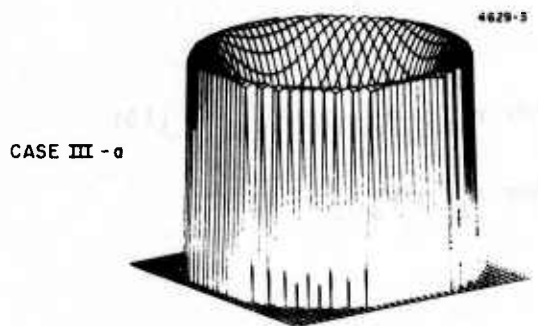CASE III-c

4629-5

CASE III-d

4629-6

Figure 8.
Three-dimensional plots of transmitter irradiance profiles that have an on-axis null initially that fills in as the beams propagate. Case III-a is a Laguerre-Gaussian mode. Case III-b is similar to Case II-b, except $|u|^2$ has no $\theta$-dependence. Case III-c is a uniform annular beam. Case III-d is an annularly-truncated Gaussian beam.
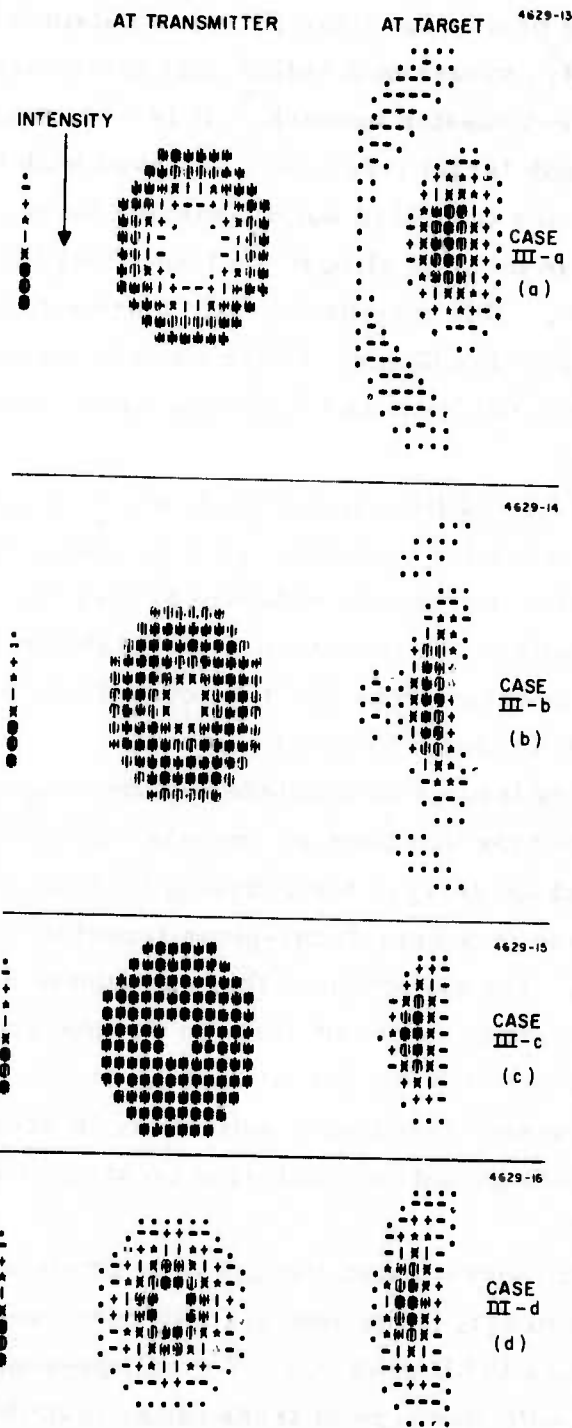
Figure 9.
Pseudo-gray scale plots of transmitter
and focal-plane (target) irradiance dis-
tributions for the three beams in Fig. 4.
A moderate amount of thermal blooming
is present in the propagation path.

41

The intensity profile for Case (III-a) is obtained by combining the $TEM_{00}$ and $TEM_{10}^{*}$ modes of a cylindrical cavity oscillating in phase opposition (Laguerre-Gaussian modes).[7] It is worthwhile to point out that, although the peak target irradiance achieved with this profile is almost twice that of the truncated solid Gaussian beam, the total laser power for this profile must be almost ten times that for the truncated solid Gaussian beam. This may be too high a price to pay for a factor of 2 increase in target irradiance. Other ways to increase target irradiance by this amount such as COAT may be more practical and efficient.

In cases (III-b) and (III-c), the peak target irradiance is also about twice the value for the truncated solid Gaussian beam, but as shown in Fig. 10, this increase is obtained at less than one-half the total input laser power of the truncated solid Gaussian beam. It is important to note, however, that this type of uniform intensity distribution is very difficult to obtain in practice.

These results lead us to conclude that most special laser modes or intensity distributions that have an on-axis null or minimum do not offer any significant advantages for reducing thermal blooming when the goal is to achieve maximum focal-plane irradiance for a given transmitter power. The exception to this conclusion occurs when the initial irradiance profile is very uniform in its nonzero regions (the uniform annulus of case (III-c), for example). It may be impractical, however, to achieve such irradiance uniformity in practice with high power lasers, so that phasefront-tailoring techniques i.e., (COAT) may be more useful.

We have also investigated the use of multiple small Gaussian beams at the transmitter. This concept was conceived and demonstrated as part of the Hughes IR&D program. We will present the results of our investigations with this type of transmitter distribution in the next report along with a comparison of uniform square and rectangular beams as well as elliptical and "ramp-distribution" beams.
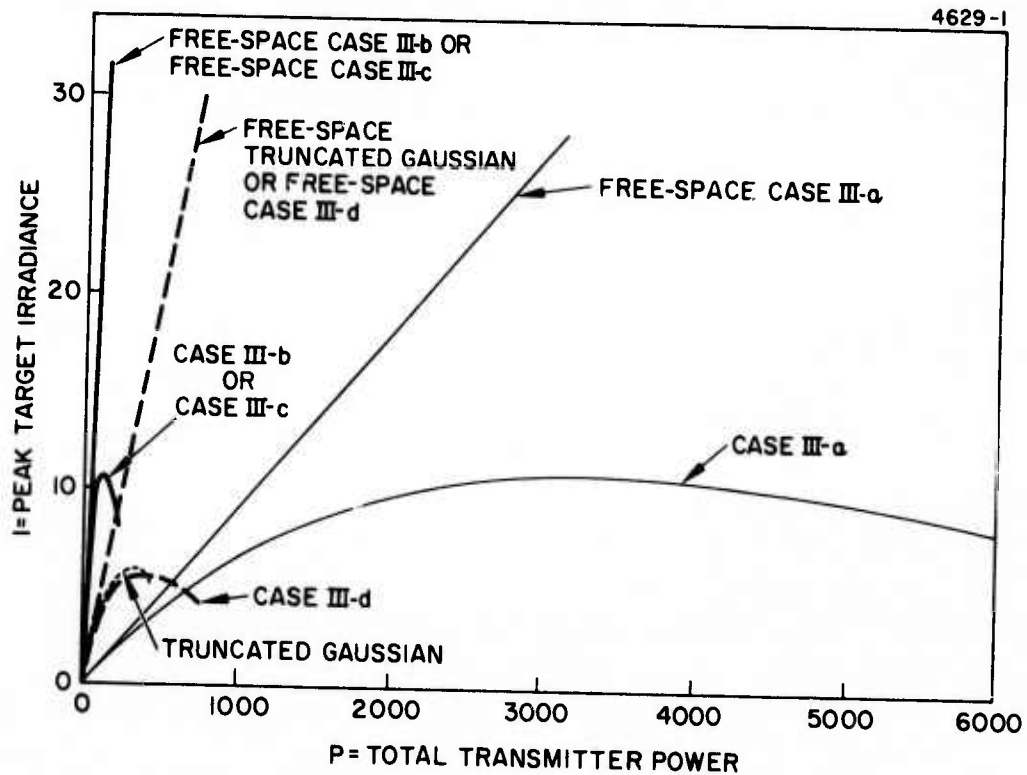
Figure 10. Peak target irradiance versus total transmitter power for the four beams in Figs. 5 and 6.

## III. PLANS FOR THE SECOND CONTRACT QUARTER

Four goals will be accomplished during the next quarter. First, we will complete the irradiance-tailoring studies. Second, we will build a Zernike-polynomial generator so that the DARPA/RADC COAT electronics can be used to produce a ZEP-COAT system. This generator consists of weighting and summing matrices, one for each polynomial. We will also construct a dither-injection unit so that the dither and correction signals can be combined on the single deformable mirror for our MOW-COAT tests (this combining function is done in the polynomial generator for ZEP-COAT). Third, we will determine whether the instabilities are caused by errors in the ZEP-COAT computer model or coding, by servo parameters which need to be modified, or by more fundamental problems with the components of the feedback signal from the Zernike polynomials. We will also investigate in detail which polynomials compensate best for blooming, when the mirror characteristics are included. Continuation of both the analytical and computer studies in the next quarter should give us a handle on optimizing the convergence characteristics of the ZEP-COAT system. Finally, the deformable mirror construction is scheduled for completion by 1 March 1976.

# REFERENCES

1. W.B. Bridges, J.E. Pearson, et al., "Coherent Optical Adaptive Techniques," RADC Reports No. RADC-TR-73-384, -74-38, -74-108, -74-187, and -75-46, (772 639), (776 814), (779 668), (783 281), (A007032).

2. J. Wallace, I. Itzkam, and J. Camm, J. Opt. Soc. Am. $\underline{64}$, 1123 (1974).

3. D.L. Fried, Appl. Opt. $\underline{13}$, 989 (1974).

4. P.B. Ulrich, J. Opt. Soc. Am. $\underline{64}$, 549 (1974).

5. L.W. Casperson and M.S. Shekhani, Appl. Opt. $\underline{14}$, 1653 (1975).

6. G.D. Boyd and J.P. Gordon, Bell Syst. Tech. J. $\underline{40}$, 489 (1961).

7. G. Goubau and F. Schwering, IRE Trans. Antennas and Propag. $\underline{AP-9}$, 248 (1961).

8. J.E. Pearson, et al., "COAT Measurements and Analysis," contract F30602-75-C-0001, RADC Reports No. RADC-TR-75-47, -75-101; Technical Report No. 3, June, 1975; Final Technical Report, Dec. 1975, (A006105), (A011707).

9. M. Born and E. Wolf, Principles of Optics, ch. 9 (Pergamon Press, 1964).

10. S.N. Bezdid'ko, So. J. Opt. Technol. $\underline{41}$, 425 (1974).

11. L.C. Bradley and J. Herrmann, Appl. Opt. $\underline{13}$, 331 (1974).

12. W.P. Brown, Jr., "Computer Simulation of Adaptive Optical Systems," Final Report on Contract N60921-74-C-0249, Sept. 1975.